dATP Elevation Induces Myocardial Metabolic Remodeling to Support Improved Cardiac Function

Ketaki N Mhatre[1,6,9], Jason D Murray[1,2,9], Galina Flint[1,9], Timothy S. McMillen[3,10], Gerhard Weber[4], Majid Shakeri[4], An-Yue Tu[1,9], Sonette Steczina[1,9], Robert Weiss[5], David J. Marcinek[11], Charles E Murry[4,6,9], Daniel Raftery[3,8,10], Rong Tian[3,8,10], Farid Moussavi-Harami[4,9,10]*, Michael Regnier[1,2,9,10]*

1. Department of Bioengineering, University of Washington, Seattle, WA 98109
2. Department of Physiology and Biophysics, University of Washington, Seattle, WA 98109
3. Department of Anesthesiology and Pain Medicine, University of Washington, Seattle, WA 98109
4. Division of Cardiology, University of Washington, Seattle, WA 98109
5. Department of Biomedical Sciences, Cornell University, Ithaca, NY 14853
6. Department of Laboratory Medicine & Pathology, University of Washington, Seattle, WA 98109
7. Department of Comparative Medicine, University of Washington, Seattle, WA 98109
8. *The Mitochondria and Metabolism Center* (MMC), University of Washington, Seattle, WA 98109
9. Institute for Stem Cell and Regenerative Medicine, University of Washington, Seattle, WA 98109
10. Center for Translational Muscle Research, University of Washington, Seattle, WA 98109
11. Department of Radiology, University of Washington, Seattle, WA

* Correspondence to mregnier@uw.edu and moussavi@uw.edu

Highlights

- Ubiquitylation-resistant variant RRB in a transgenic mice model (TgRRB) elevates dATP level up to 1% (of the total ATP pool) in the heart and improves function.
- TgRRB-CMs show greater basal oxygen consumption due to changes in myosin state by dATP.
- TgRRB-CMs respond to elevated function with a metabolic shift, such that there are higher pools of oxidative metabolites, with elevated OXPHOS, FAO, and energy reserve.
- Long-term mitochondrial remodeling may occur to accommodate for the higher energy demands of the high functioning TgRRB-CMs.

Abstract

Hallmark features of systolic heart failure are reduced contractility and impaired metabolic flexibility of the myocardium. Cardiomyocytes (CMs) with elevated deoxy ATP (dATP) via overexpression of ribonucleotide reductase (RNR) enzyme robustly improve contractility. However, the effect of dATP elevation on cardiac metabolism is unknown. Here, we developed proteolysis-resistant versions of RNR and demonstrate that elevation of dATP/ATP to ~1% in CMs in a transgenic mouse (TgRRB) resulted in robust improvement of cardiac function. Pharmacological approaches showed that CMs with elevated dATP have greater basal respiratory rates by shifting myosin states to more active forms, independent of its isoform, in relaxed CMs. Targeted metabolomic profiling revealed a significant reprogramming towards oxidative phosphorylation in TgRRB-CMs. Higher cristae density and activity in the mitochondria of TgRRB-CMs improved respiratory capacity. Our results revealed a critical property of dATP to modulate myosin states to enhance contractility and induce metabolic flexibility to support improved function in CMs.

Keywords: dATP, Myosin activator, Cardiac DRX, Contraction, Cardiomyocyte metabolism, Mitochondrial remodeling

Graphical abstract

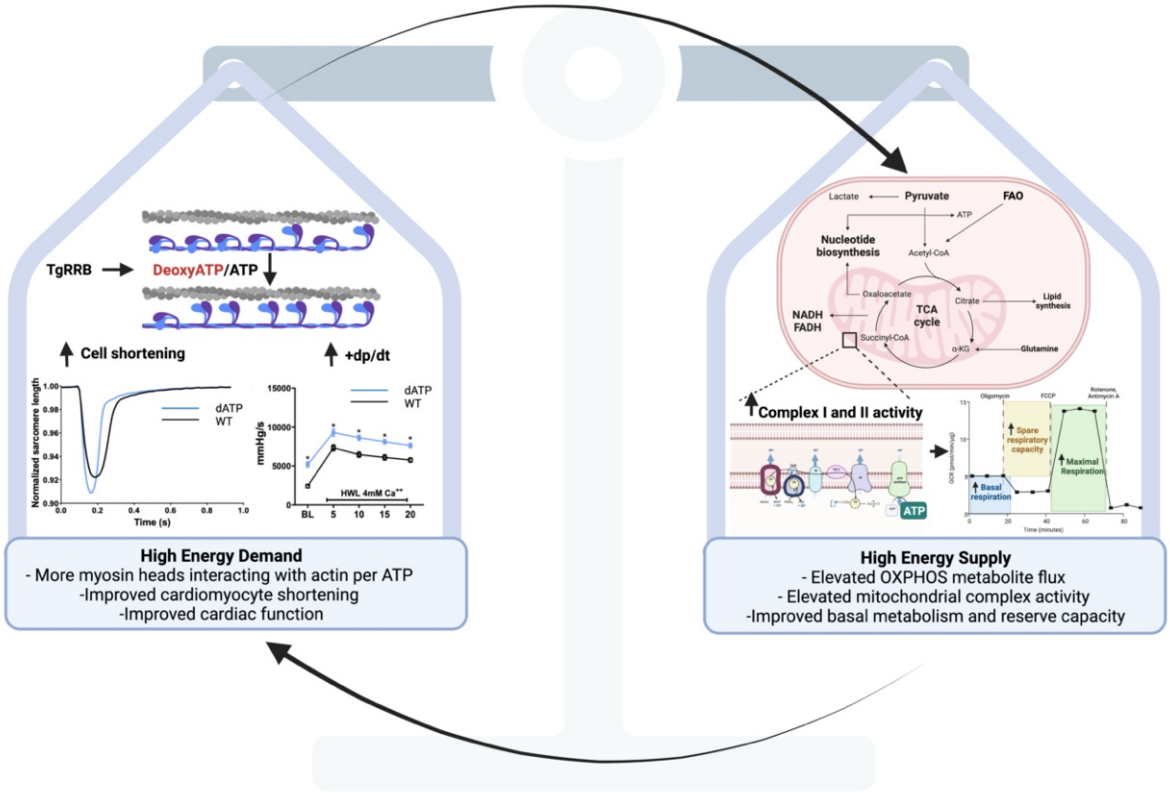

Introduction

Heart failure (HF) is a clinical diagnosis based on a constellation of symptoms due to impaired ventricular filling or ejection of blood, the latter of which is dependent on actin-myosin cross bridge cycling during systolic muscle contraction. There are also dramatic changes in cardiac metabolism in the failing hearts, such as loss of metabolic flexibility and energy deficiency[1]. Traditional inotropic agents exert their effect by modulating calcium signaling pathways, but their use is associated with poor patient outcomes[2]. All the currently approved positive inotropic drugs increase intracellular cyclic adenosine monophosphate (cAMP) along with cardiac output at the expense of energetic efficiency, which can lead to maladaptive remodeling and arrhythmia[3]. Hence, there is a need for targeted therapies to reduce morbidity and mortality[4–7]. Direct targeting of the myofilament is desirable but many compounds that increase contraction may impair relaxation and cardiac enegetics[8,9]. An ideal therapeutic

agent for the treatment of systolic dysfunction would be to improve systolic function and cardiac metabolism without impairing diastolic function.

We have previously reported that the naturally occurring nucleotide dATP is an effective molecule that improves cardiac contractility. dATP binds to cardiac myosin with a similar affinity as ATP, and it enhances the rate and magnitude of both force development and relaxation of cardiac muscle from rodents, porcine, canine, and human tissues[10–15]. This occurs by increasing myosin recruitment[16] and the dynamics of myosin-actin cross bridge cycling[17,18]. Our recent studies showed that enhanced myosin-binding with dATP (vs ATP) occurs via increasing electrostatic interactions between myosin and actin[19,20], as well as by augmented recruitment of myosin from a low activity state (SRX) on the thick filament backbone to a higher activity state (DRX) where one or both heads are free to interact with thin filament[21]. In skeletal muscle, we provided evidence that elevated dATP maintains myosin S1 heads in a position closer to thin filaments during relaxation and that this can facilitate subsequent contraction cycles[22]. Thus, dATP enhancement of cardiac muscle function occurs via multiple mechanisms.

RNR is the enzyme that converts nucleotides to deoxynucleotides, including dATP. Overexpression of RNR using either a transgenic mouse model (TgRR) or viral vectors, have shown that dATP levels can be increased from the baseline of <0.1% to ~ 1% of the ATP pool in cardiomyocytes (CMs). This, in turn, increases CM contraction, left ventricular (LV) developed pressure and both the rate of pressure development (+dP/dt) and decline (-dP/dt) to improve heart function in both small and large animal models of HF[23–25]. RNR is a hetero-tetramer consisting of two subunits: a large subunit of RRM1 dimer which contains the catalytic site, and one of two isoforms of a small subunit, RRM2 or RRM2B, which associate together to form RNR holoenzyme[26,27]. Over-expression of RRM2 was highly effective in improving cardiac function, via elevation of dATP, in our earlier transgenic model (TgRR). However, this subunit is tightly regulated by the ubiquitin-proteasome system across the cell cycle and thus may pose challenges for its stable expression in post-mitotic cells like CMs[28–30]. In this study, we investigated proteolysis-resistant isoforms of RRM2, RRM2B, [28,30] to stably elevate dATP levels in CMs and improve its function.

Recent studies have shown that modulation of the myosin state (based on ATPase turnover) via disease-related mutations[31] not only alters contractile function at the cellular and organ level

110 but also cellular energetics[32]. These mutations can augment recruitment of myosin from a low
111 activity state (SRX) on the thick filament backbone to a higher activity state (DRX) where one or
112 both heads are free to interact with thin filament[21] and can contribute to the observed increase
113 in the energy cost of force generation[32,33]. This can result in energy deficient CMs leading to
114 enhanced ROS production, mitochondria damage, and altered mitochondrial content, cristae,
115 and respiratory complexes. This, in the long-term, causes myocardial energy deprivation in
116 cardiomyopathies[34]. Thus, myosin states and their effect on contractile activity can modulate
117 cardiac metabolism and mitochondria function and it would be important to study the long-term
118 effect of myotropes[35], drugs that directly modulate the contractile machinery , like dATP in this
119 respect.
120
121 In the current study, we demonstrate that elevating dATP by overexpression of RRM1 and
122 RRM2B elevates LV systolic and diastolic function. dATP elevation has shown to improve
123 function via increase of cross bridge recruitment and binding to actin (crossbridge formation)
124 and crossbridge cycling[16–18,20]. This results in higher basal ATPase turnover, leading to
125 higher energy demands. Current study suggest that cellular metabolism adapts to greater
126 oxidative capacity and mitochondrial remodeling thereby possibly maintaining (d)ATP supply
127 and energetic reserves in high functioning CMs with chronically elevated dATP.
128

129 Results

130

131 **RNRB overexpressing mice have elevated dATP and improved systolic and diastolic**
132 **function**

133
134 Here we studied a transgenic mouse line (TgRRB) that globally overexpresses two subunits of
135 ribonucleotide reductase: the large subunit RRM1 and the p53-inducible isoform of the small
136 subunit, RRM2B. Wild-type littermates were used as controls.
137
138 We used high-performance liquid chromatography-mass spectrometry (HPLC-MS/MS) to
139 measure total dATP (along with other dNTPs, Fig. S2a) and ATP content. The ratio of dATP to
140 ATP was significantly elevated for hearts of 4-month-old RNRB versus WT littermate mice in the
141 myocardium (Fig. 1a; RNRB = 0.91±0.07% vs WT = 0.01±0.002%), in isolated CMs (Fig. S2b)
142 and in isolated mitochondria (Fig. S2c).

143

144 *In vivo* cardiac function was first assessed by echocardiography (Table S1). TgRRB mice had
145 significantly greater LV fractional shortening and ejection fraction (Fig. 1b, Table S1). This
146 occurred without difference in heart weight (Fig. S1), systolic ejection time (SET) and LV end-
147 diastolic dimensions (Table S1) between TgRRB and WT hearts. The left-ventricular myocardial
148 performance index (LV MPI), which reflects both systolic and diastolic function was significantly
149 lower (indicating improved performance) in TgRRB mice as compared to WT. The gain in
150 systolic function did not result in diastolic dysfunction as E/E', a measure of LV filling pressure,
151 and isovolumic relaxation time (IVRT), a measure of LV relaxation, were unchanged in the two
152 groups (Table S1). Thus, the elevation of cytosolic [dATP] enhances systolic function without
153 contributing to cardiac hypertrophy (Fig. S1) or impairing diastole (Fig. 1 and Table S1)[23].
154

155 To determine the effect of elevated dATP on cardiac function we used isolated Langendorff-
156 perfused hearts to measure the *ex vivo* LV hemodynamics at baseline and with a high workload
157 challenge. In paced hearts LV developed pressure (LVDP) product and both positive (+dP/dt)
158 and negative (-dP/dt) rates of pressure development were greater for hearts from TgRRB vs WT
159 mice (Fig. 1c, d, e). Interestingly, the rate-pressure product (RRP), a measure of cardiac output
160 (Fig. S3b), was also greater for hearts from TgRRB mice. Myocardial responsiveness to high
161 workload was elicited by elevating Ca^{2+}. LVDP increased in both TgRRB and WT hearts, as did
162 +dP/dt, in agreement with earlier findings that RNR overexpression does not compromise the
163 heart's ability to increase output[23,36] (Fig. S3d). Although mean LVDP and rate of pressure
164 development were significantly higher, heart rate was slightly lower in unpaced TgRRB hearts
165 (Fig.S3d, e). This resulted in similar rate pressure product between the two groups under higher
166 workload conditions. Diastolic performance (-dP/dt) was comparable between the groups in
167 response to the high-calcium challenge (Fig. S3h).
168

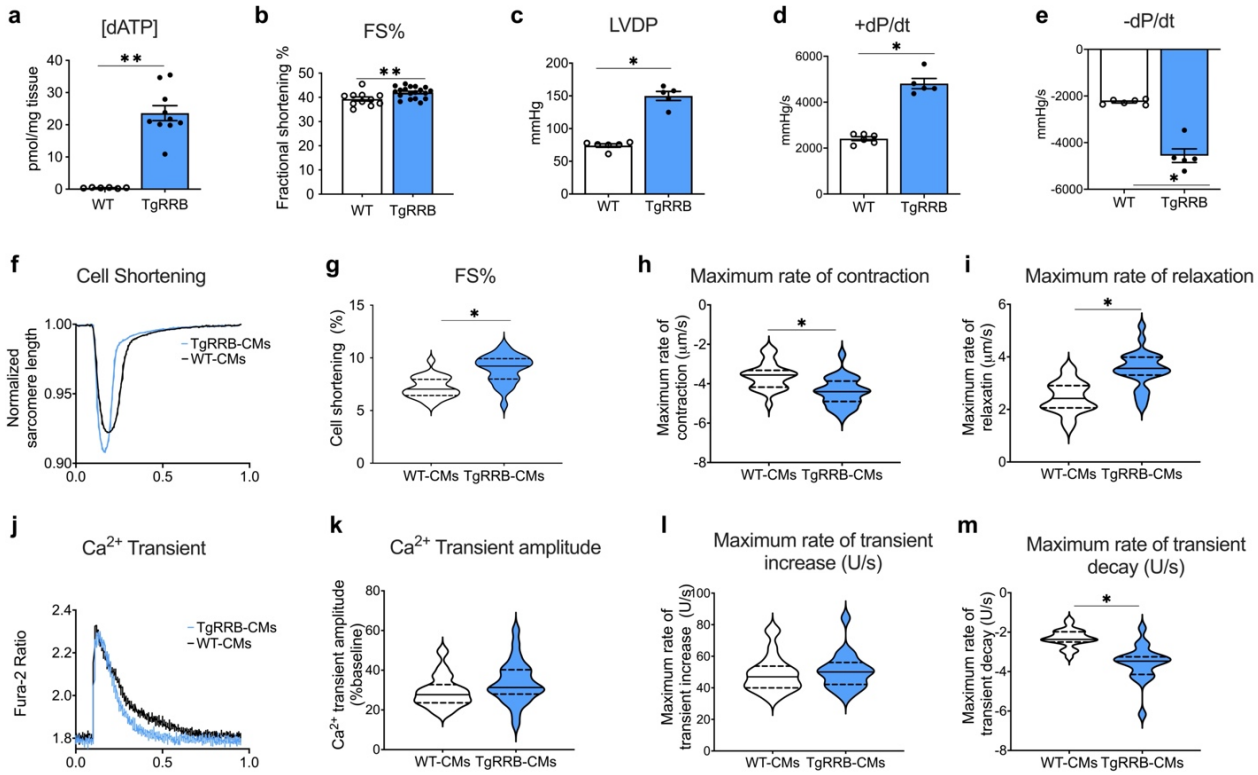

Fig. 1. TgRRB mice have elevated dATP and improved systolic and diastolic function. (a) [dATP] mass spectrometry measurements from the myocardium. (b) Echocardiogram measurements FS: Fractional Shortening. (c-e) Baseline contractility in perfused isolated hearts LVDP: Left-ventricular developed pressure, +dP/dt: maximum rate of pressure development in contraction, -dP/dt: maximum rate of pressure development in relaxation. Measurements of cell shortening and Ca transients in isolated mouse CMs. (f) Representative traces of sarcomere length (g) Fractional Shortening (h) Maximum rate of contraction (i) Maximum rate of relaxation (j) Representative traces of calcium transients (k) Calcium Amplitude (Fura-2 ratio-%baseline) (l) Maximum rate of Ca transient increase (m) Maximum rate of Ca transient decay. a-b: N = 6-8 mice per group. c-e: N = 6-7 mice per group. f-m: N = 6-7mice per group, n≥70 cells per group. All data are presented as mean ± SEM. P values were determined by unpaired, two-tailed, Student T test, *p ≤ 0.05, **p ≤ 0.01.

To determine the cellular basis of increased LV function, we measure single-cardiomyocyte (CM) Ca^{2+} transients and the resulting contractility. TgRRB-CMs exhibited significantly greater fractional shortening and maximum rates of contraction and relaxation as compared to WT cells (Fig. 1f). There was no significant difference in Ca^{2+} transient amplitude or time to peak amplitude in CMs from TgRRB versus WT mice and no change in baseline (resting) Ca^{2+} (Fig. 1j and Table S2). However, the rate of intracellular Ca^{2+} decay was greater in TgRRB-CMs. An increase in SERCA activity could explain the increased decay rate of the Ca^{2+} transient. However, there was no significant difference in sarcoplasmic reticulum Ca^{2+} store between the two groups. Thus, suggesting a different mechanism underlying faster Ca^{2+} decay observed in CMs with elevated dATP. In summary, all methods of increasing dATP enhanced contraction and relaxation in CMs.

Further, we examined the effect of chronic elevation of dATP on the sarcomeric protein function. We checked the phosphorylation state of sarcomeric protein - MyBP-C, Desmin, troponin T, troponin I, and MLC-2 in isolated myofibrils from hearts of both the groups (Fig. S4). There was no significant difference between the phosphorylation state of these sarcomeric protein which are possible modifiers of contractile properties in myocardium. Further, we studied Force pCa relationship and passive tension measurements in skinned cardiac muscle preparations (Fig. S6) from both the groups. Force generated at series of %stretch (sarcomere length) didn't differ suggesting no difference in sarcomere elasticity within the groups (Fig. S6d)[14,37]. It is an indirect measurement of titin isoforms and its phosphorylation regulating the passive stiffness[38], suggesting no changes in the model of dATP chronic elevation. However, TgRRB trabeculae generated significant greater normalized force at pCa 4 than WT independent of dATP elevation (Fig. S6a, b). This suggest that even though we didn't find difference in phosphorylation status of the sarcomeric protein, there is a possible myofilament adaption in myosin due chronic elevation of dATP, where more myosin heads interacting or interacting more strongly with actin even in absence of dATP elevation[20,22]. Nonetheless, TgRRB skinned trabeculae did respond to the dATP treatment like WT suggesting that the sensitivity to dATP is maintained in TgRRB trabeculae (Fig. S6d).

Elevation of cardiomyocyte dATP leads to an increase in oxidative respiration capacity via increased myosin activation.

220 In disease state of heart, there is a correlation between elevated crossbridge turnover rate and
221 increased energetic cost of myocardial contraction[33]. Protein biochemistry measurements
222 have shown this can also occur in resting cardiac muscle. The portion of myosin heads in
223 sarcomeres in the disordered-relaxed (DRX) state (Fig. 3a) have a relatively high ATPase
224 activity (~0.03 s^{-1}) compared with the remainder of heads sequestered on the thick filament
225 backbone in the super-relaxed (SRX) state with very low ATPase activity rates (~0.003 s^{-1})[39].
226 We recently reported that for myofibrils in solutions with 100% dATP, the SRX state is
227 completely depopulated[40], resulting in significant increase in myofibrillar ATPase activity.
228 However, it is unclear whether and how much ATPase in relaxed myofibrils is affected when the
229 dATP content is ~1% of the total ATP pool, and how this may affect CM metabolism.
230
231 Thus, to determine how elevated dATP on the energetics of CMs, we measured oxygen
232 consumption rate (OCR) of the TgRRB-CMs. These measurements were done on isolated cells
233 cultured in assay medium with pyruvate and glucose following sequential addition of oligomycin
234 (an inhibitor of ATP synthase), Carbonyl cyanide-p-trifluoromethoxy phenylhydrazone (FCCP,
235 mitochondrial oxidative phosphorylation uncoupler), Antimycin A and Rotenone (mitochondrial
236 electron transport chain inhibitor).
237

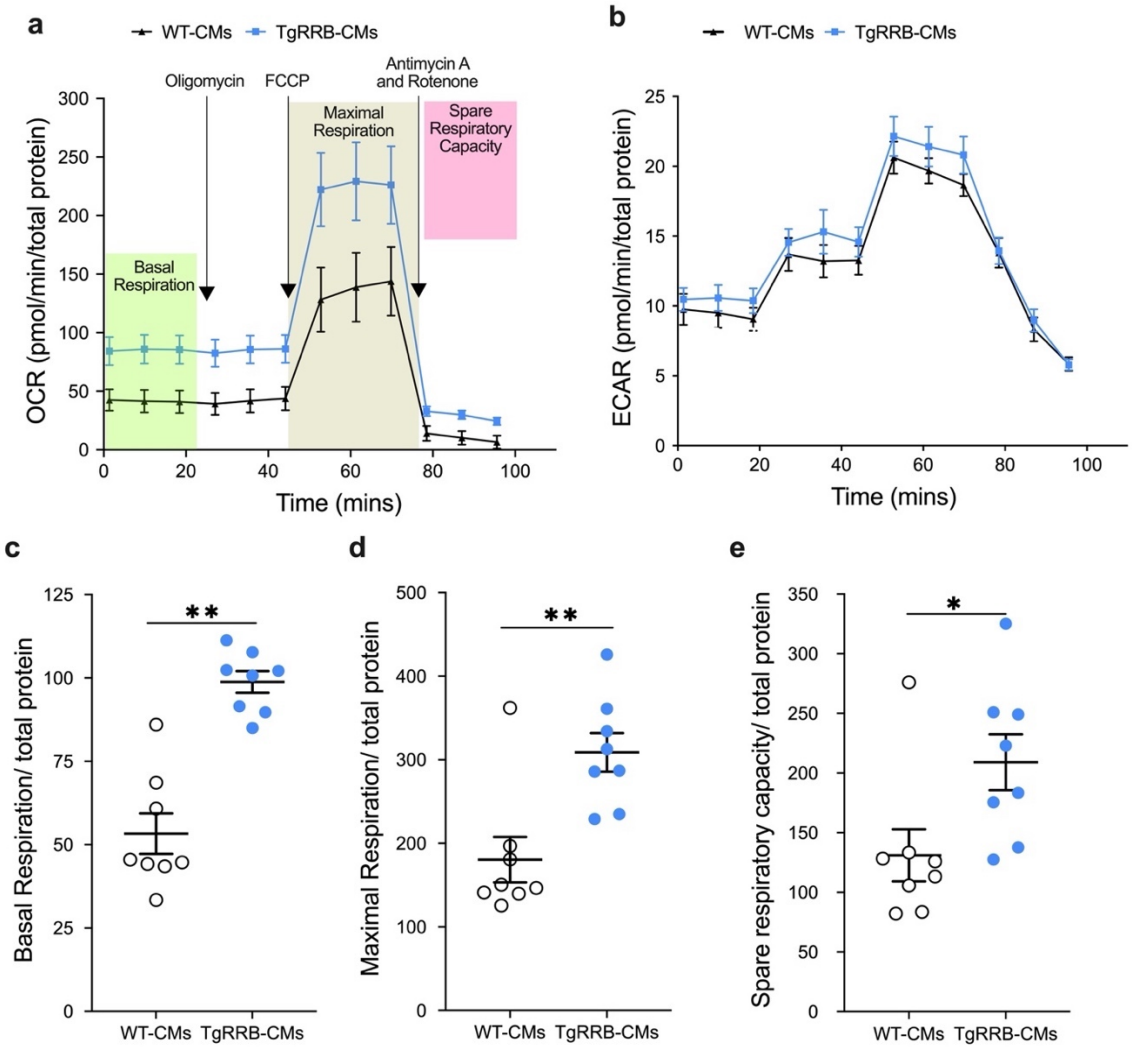

Fig. 2. Assessment of cellular bioenergetics in TgRRB-CMs. Oxygen consumption rate (OCR) was measured on a standard Seahorse Mito stress test. (a) Representative OCR plot of CMs isolated from TgRRB vs WT mice (SD). (b) Representative ECAR plot of adult mice CMs isolated from TgRRB vs WT mice (SD). (c) Basal OCR (d) Maximal OCR and (e) Spare respiratory capacity normalized to the total protein. (c-d) N=8 mice per group, n≥3 technical replicates / animal. All data are presented as mean ± SEM. P values were determined by unpaired, two-tailed, Student T test, *P<0.05, **P<0.01.

Basal respiration of TgRRB-CMs was approximately double that of cells from WT mice (Fig. 2c). TgRRB-CMs also had a 1.5-fold greater FCCP-stimulated maximal respiratory capacity (Fig. 2d). Subsequently, TgRRB-CMs show significantly elevated spare respiratory capacity (Fig. 2e). Spare respiratory capacity serves the increased energy demands when cells are subjected to stress, thereby maintaining cellular and organ function, cellular repair, or detoxification of

252 reactive species[41]. Thus, TgRRB-CMs may perform better under high energy demands.
253 Nevertheless, there was no significant difference between the groups in the extracellular
254 acidification rate (ECAR), a surrogate for glycolytic activity (Fig. 2b). In CMs, factors such as cell
255 size, sarcomere length, and beat rate can affect mechanical function as well as the oxygen flux
256 and bioenergetics. The TgRRB-CMs did not exhibit differences in cell morphology or sarcomere
257 length compared to WT-CMs (Fig. S1b).
258
259 Basal respiration is usually strongly controlled by ATP turnover via myosin ATPase, SERCA
260 ATPase and other ion pumps and possibly be reflective of the higher cell shortening in TgRRB-
261 CMs (Fig. 1f). Interestingly, our assessment of SERCA activity in mice cardiac tissue did not
262 show a preference for ATP or dATP as substrate (Fig. S5) and we found no difference in
263 sarcoplasmic reticulum Ca^{2+} load between TgRRB-CMs and WT-CMs (Table S2), suggesting
264 that SERCA ATPase may not contribute to the basal respiration of TgRRB-CMs. Thus, these
265 data suggest that the dATP elevation affects cellular bioenergetics, likely via modulation by
266 myosin ATPase activity, as we have recently shown[21].
267
268 To address whether higher OCR was due to dATP mediated changes in the myosin SRX/DRX
269 ratio[21], we treated TgRRB-CMs with Mavacamten (a selective myosin-motor inhibitor).
270 Mavacamten is known to reduce myosin available for cross bridge cycling by recruiting myosin
271 into the SRX state, leading to lower ATPase activity (Fig. 3)[42]. Acute treatment (1h) of
272 Mavacamten reduced basal respiration of the TgRRB-CMs to WT-CMs levels (Fig. 3c) but did
273 not affect the maximal respiratory capacity (Fig. 3d), thus supporting the idea that elevation in
274 basal OCR is mainly due elevated myosin ATPase activity in TgRRB-CMs [40].
275
276 Importantly, in addition to basal respiration, mitochondria-dependent FCCP- induced -maximal
277 oxygen flux was higher in TgRRB-CMs (Fig. 3d). The FCCP stimulated OCR suggests
278 significant differences in the maximal mitochondrial capacity and electron transport chain (ETC)
279 activity between TgRRB-CMs and WT-CMs, and these differences were not affected by
280 Mavacamten. Thus, the mitochondria in TgRRB cells may have independent mechanisms of
281 compensation (Fig. 2d and e) with elevation of dATP, improving spare respiratory capacity of
282 these CMs.
283
284

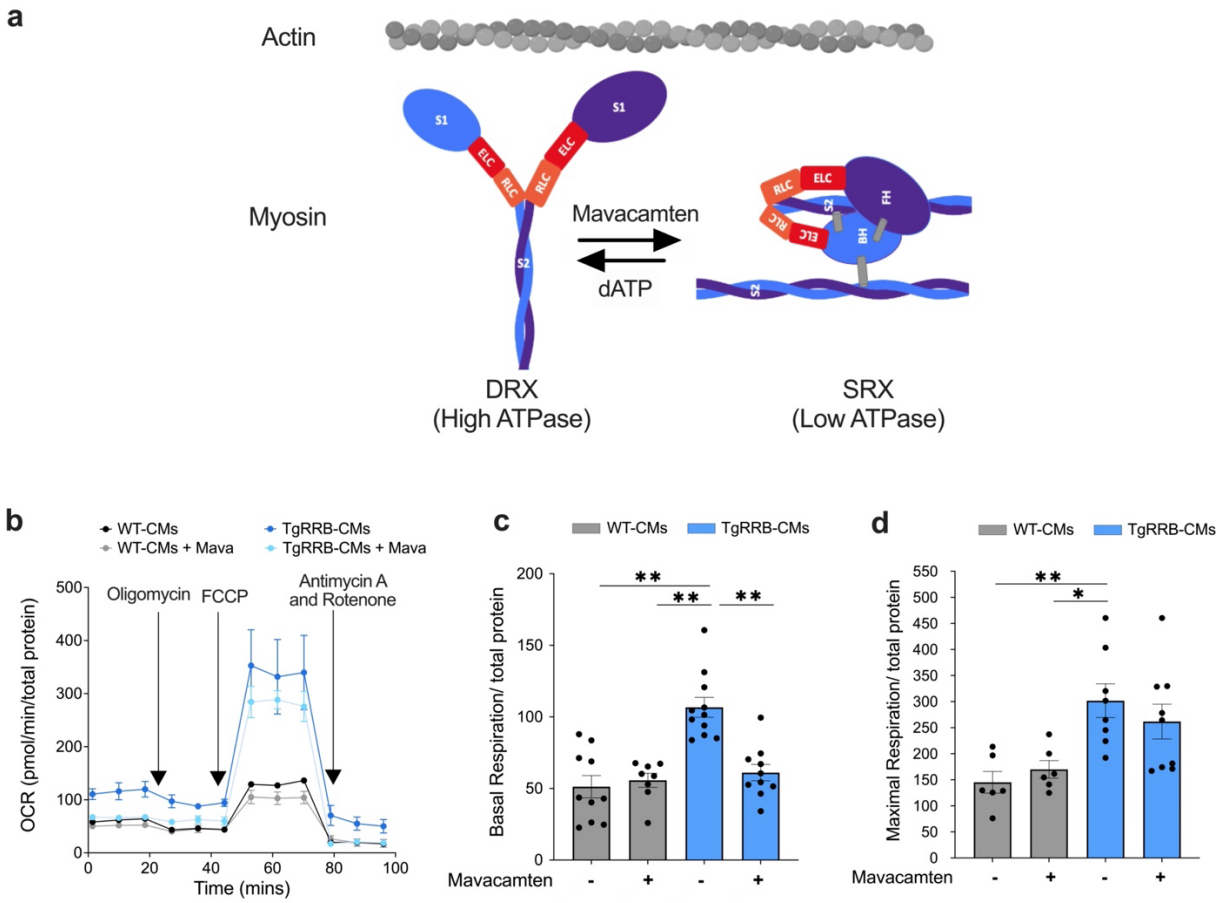

Fig. 3 Constitutive dATP elevation leads to an increase in basal respiration via modulating myosin activation state (a) The myosin ATPase states (DRX and SRX) can be modulated by Mavacamten and dATP[21]. ELC: essential light chain: RLC: regulatory light chain, BH: blocked (S2) head, FH: free (S2) head. Actin filament is shown in grey. Assessment of oxygen consumption rate (OCR) was performed with and without 1h treatment of Mavacamten (Mava, 3 μM) on adult mice CMs isolated from TGRRB vs WT mice (b-d). (b) Representative OCR plot, (c) Basal OCR (d) Maximal OCR normalized to the total protein. N=3 animals/group, n≥3 technical replicates / animal. All data are presented as mean ± SEM. P values were determined by ordinary one-way ANOVA with multiple comparison, *P<0.05, **P<0.01.

Metabolomics profiling reveals that TgRRB-CMs have elevated oxidative phosphorylation (OXPHOS) metabolite levels.

301 We performed metabolomic analyses to understand the metabolic consequences of long-term
302 elevation of dATP and the subsequent enhanced myosin activity. Targeted metabolomic
303 analyses by LC-MS of isolated CMs from TgRRB mice and age-matched WT mice at 5-7
304 months of age measured 184 metabolites (Fig. S8). PCA of all 184 metabolites clearly separate
305 the profiles of TgRRB-CMs (blue) from control WT-CMs (grey) (Fig. S8). The targeted analyses
306 allowed assessment of altered pool sizes of intermediates relevant to glycolysis, the
307 tricarboxylic acid cycle (TCA), fatty acid oxidation (FAO), and the pentose phosphate pathway
308 (PPP). In the TgRRB-CMs there was a significant increase in pyruvate and all the TCA cycle
309 intermediates, and a significant reduction in lactate/pyruvate ratio (Fig. 5a), suggesting a shift
310 towards higher levels of pyruvate entering the TCA cycle. There were no differences in
311 glycolytic intermediates (Fig. 4). Since there were lower levels of most PPP metabolites
312 compared to WT-CMs, it suggests rerouting towards glucose oxidation in TgRRB-CMs. Amino
313 acids such as phenylalanine, tryptophan, glutamate, serine, isoleucine, and glycine were more
314 abundant in TgRRB-CMs compared to WT-CMs (Fig. 5d), and there was a trend toward the
315 accumulation of citrulline, suggesting activation of the urea cycle and amino acid anaplerotic
316 feeding of the TCA cycle. Thus, in TgRRB-CMs, there was an overall increase in OXPHOS
317 compared to WT-CMs.

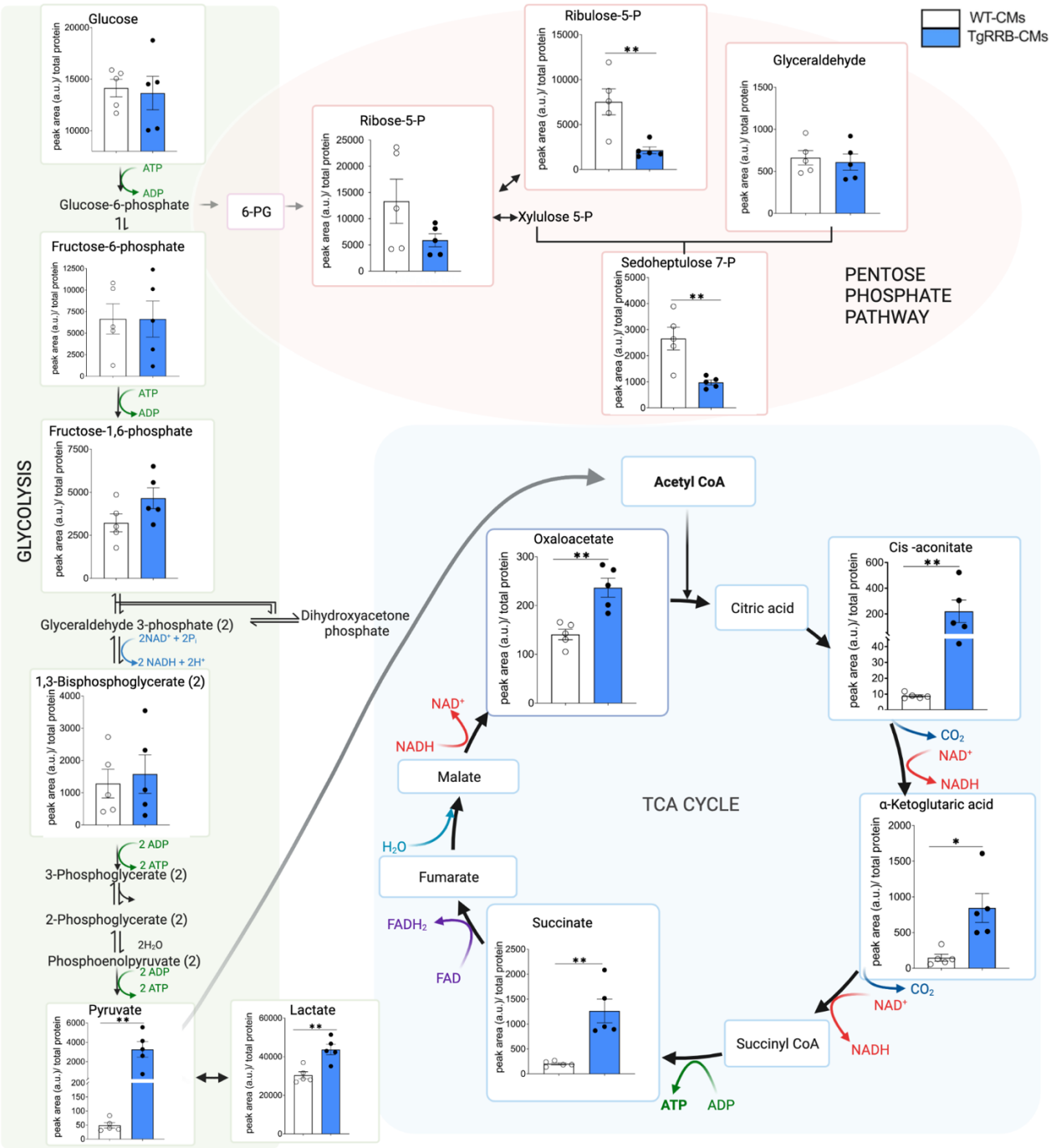

Fig. 4. Pathway analysis of metabolites involved in Glycolysis, Pentose phosphate pathway, TCA cycle, in **isolated CMs from TgRRB vs WT** Pathway analysis obtained from mass spectrometry-based metabolomics. N=5 animals/group. All data are presented as mean ± SEM. P values were determined by unpaired, two-tailed, Student T test, *P<0.05 **P<0.01. (Created with Biorender.com)

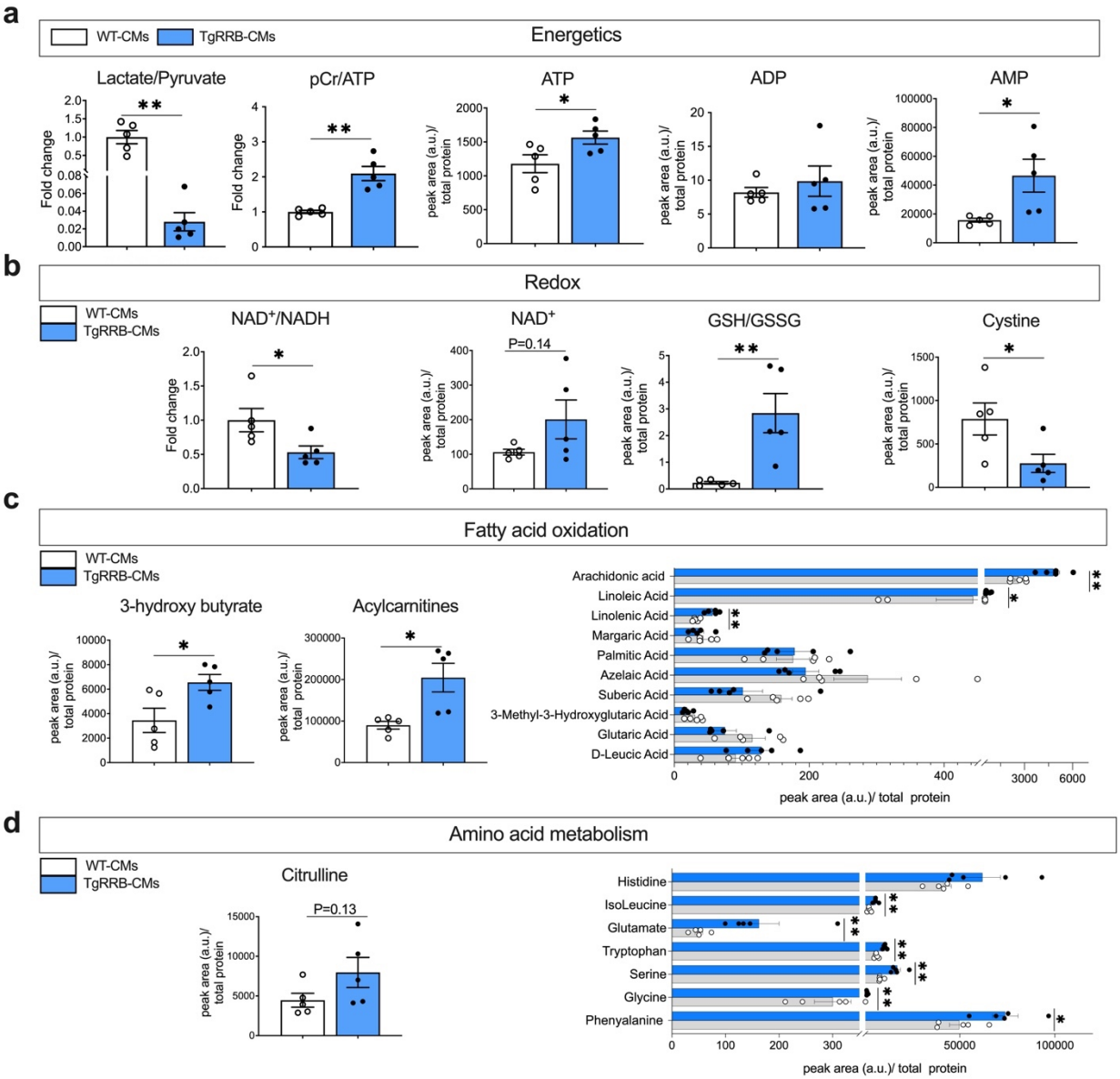

Fig. 5. dATP elevation alters cellular metabolism and energetics. Mass spectrometry assessment of cellular metabolites involved in (a) Energetics: Lactate/Pyruvate fold change, phosphocreatine (pCr)/ATP fold change normalized to WT-CMs, ATP, ADP and AMP abundance in TgRRB -CMs vs WT-CMs (b) Redox: NAD^+/NADH fold change, GSH/GSSG Fold change normalized to WT-CMs, NAD+ and Cystine abundance in TgRRB -CMs vs WT-CMs (c) Fatty acid oxidation: 3-hydroxy butyric acid, acylcarnitine and free fatty acids abundance in TgRRB -CMs vs WT-CMs (d) Amino acid metabolism: Citrulline and amino acids abundance in TgRRB -CMs vs WT-CMs. N= 5 animals per group. All data are presented as mean ± SEM. P values were determined by unpaired, two-tailed, Student T test, *P < 0.05 **P<0.01.

336
337
338 Stimulation of OXPHOS in the TgRRB-CMs is also evident from the NAD^+/NADH and
339 phosphocreatine (pCr) /ATP ratios as compared to WT-CMs (Fig. 5a, b). The latter was due the
340 phosphocreatine levels being raised more than the modest increase in ATP content in
341 transgenic CMs. Interestingly, there were also significantly greater AMP levels in TgRRB-CMs
342 (Fig. 5a). Overall, therefore, TgRRB-CMs have an oxidative metabolic profile that supports the
343 observed higher respiration rate.
344
345 In healthy myocardium, oxidative stress via OXPHOS is tightly counterbalanced by reducing
346 agents. In TgRRB-CMs, we found that the metabolites involved in the endogenous antioxidant
347 defense mechanism, such as lactate and glutathione (GSH), were significantly higher (Fig. 5b).
348 Oxidized cysteine (cystine), a marker for oxidative stress, was reduced. Thus, greater levels of
349 protective antioxidant metabolites were found in TgRRB-CMs.
350
351 TgRRB-CMs also appear to have increased fatty acid metabolism, with greater levels of 3-
352 hydroxybutyric acid (more than 1.5-fold) and intermediate products of oxidative decomposition
353 of fatty acids (Fig. 5c). These findings are suggestive of increased ketone body metabolism and
354 FAO in the TgRRB versus WT-CMs. Compared to WT-CMs, TgRRB-CMs were also enriched
355 with acylcarnitine and free fatty acids (especially polyunsaturated fatty acids like linolenic and
356 arachidonic acids), consistent with an elevated beta-oxidative capacity of TgRRB-CMs to utilize
357 fatty acids as an energy source (Fig. 5c).
358
359 Overall, the metabolomic analysis suggests that TgRRB-CMs exhibit a significant metabolic shift
360 towards increased oxidative metabolism, combined with greater phosphocreatine kinase and
361 high energy phosphates, ultimately improving the energetics of TgRRB-CMs (Fig. 4, 5).
362
363 **TgRRB-CMs have enhanced mitochondrial function compared to WT-CMs.**
364
365 We next sought to characterize whether the metabolic and energetic differences in TgRRB-CMs
366 versus WT-CMs were associated with changes in cardiac mitochondria. Increased maximal
367 respiration of TgRRB-CMs could occur via increased mitochondria biogenesis or increased
368 activity of existing respiratory chain proteins. To explore this, we studied regulators of cell
369 energetics, mitochondrial content, morphology, and function (Fig. 6).

370

371 The expression analysis of genes involved in the regulation of mitochondria biogenesis and cell
372 energetics, such as PGC1β (peroxisome-proliferator–activated receptor-γ-coactivator 1 β),
373 TFAM (transcription factor A were greater in TgRRB hearts suggesting that there is greater
374 OXPHOS gene expression[43,44] (Fig. S10). Citrate synthase activity analysis showed a trend
375 for higher levels in TgRRB-CMs compared to WT-CMs (Fig. 6a). Nonetheless, mitochondrial
376 content, determined via the mtDNA to nuclear DNA ratio, was not significantly different (Fig. 6b).
377 We next examined mitochondrial ultrastructure using transmission electron microscopy.
378 Mitochondrial number, size, aspect ratio were not different from WT group (Fig. 6d, e, g).
379 However, mitochondrial cristae density was significantly higher (38.4 % ± 0.14) in TgRRB heart
380 tissue as compared to WT, suggestive of an enhancement in the ETC complex situated on
381 cristae (Fig. 6f). Overall, these measurement suggest a potential increase of mitochondrial
382 turnover activity and quality control in TgRRB hearts[43].
383

384 A relatively higher ETC content may be elevating the oxidative capacity of the mitochondria in
385 TgRRB-CMs. We examined the overall mitochondrial activity and function of the electron
386 transport chain (ETC) proteins in TgRRB-CMs. A standard Seahorse Mito stress test was used
387 to measure oxygen flux in response to ETC complex inhibitors in sequence, to parse out
388 complex- (es) whose activity was affected (Fig. 6h, i)[45]. TgRRB-CMs had significantly greater
389 CI and CII activities compared to WT-CMs (Fig. 6j). We further confirmed higher levels of
390 complex I (CI) and II (CII) proteins in TgRRB-CMs compared to WT-CMs (Fig. 6k, l). Together,
391 these results suggest that chronic elevation of dATP improves mitochondrial respiration via
392 elevated expression and activity of CI and CII activity, fueled by elevated OXPHOS (NADH and
393 FADH2) in the TgRRB versus WT-CMs.

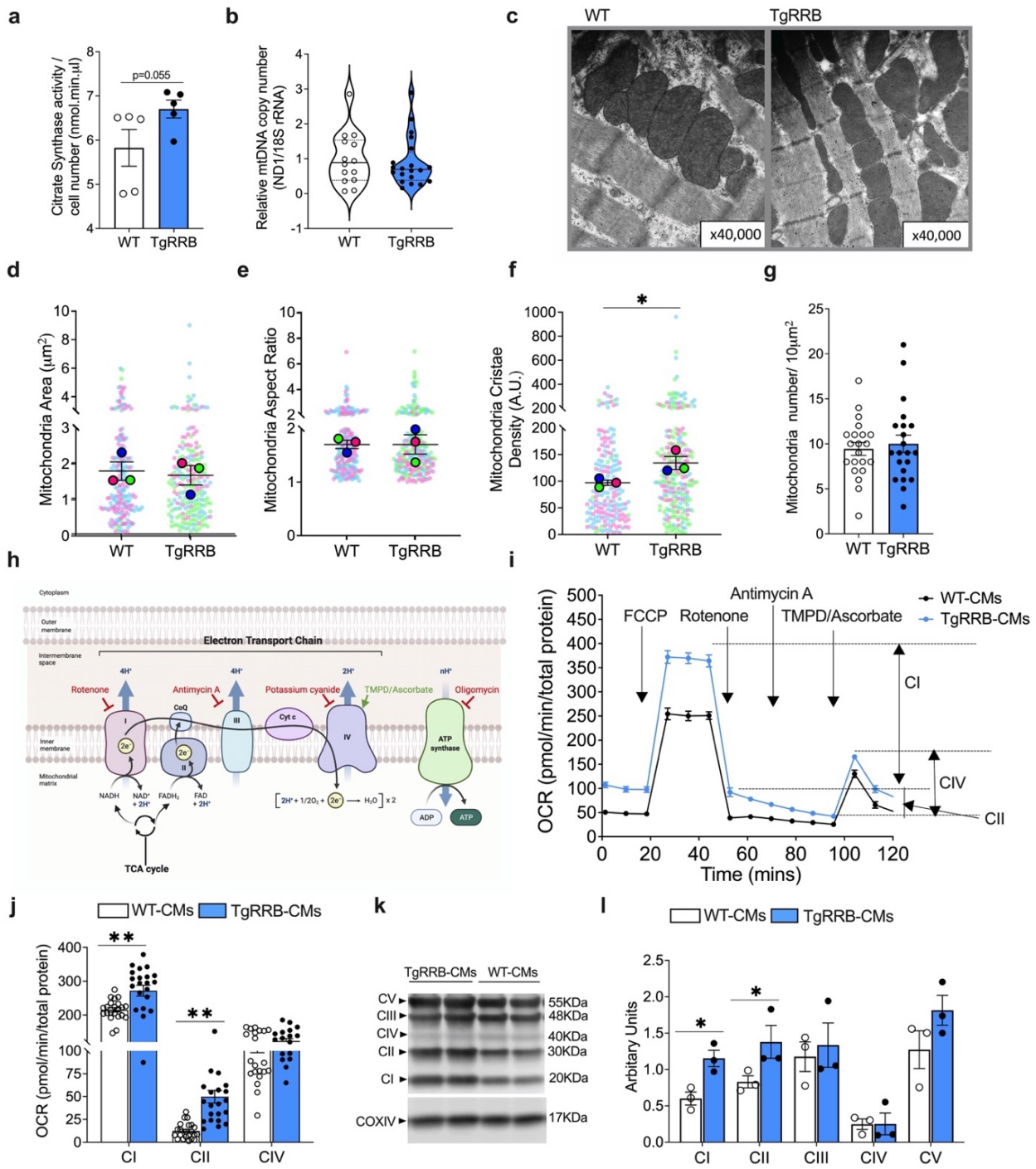

Fig. 6. The mitochondrial structure and function in TgRRB-CMs and WT-CMs. (a) Citrate synthase (CS) activity (N=5 animals/ group) (b) Relative mitochondrial DNA copy number. Mitochondrial DNA (ND1; mitochondria-encoded NADH dehydrogenase 1 gene; mtDNA) was measured relative to 18S rRNA (nucleus-encoded gene; nDNA) as the control (c) Representative electron photomicrographs of mitochondria at a magnification of x40,000.

400 Scatter plot showing morphometric analysis (X40,000) of sarcomeric (d) mitochondria area, (e)
401 aspect ratio, (f) cristae density with solid symbols as average per animal. X8000 images were
402 analyzed for (g) average mitochondria number per 10μm^2 per animal. (h) Schematic of different
403 compounds targeting Complex I (CI), Complex III (CIII), Complex IV (CIV) and ATP synthase.
404 (i) Representative OCR plot with the application of compounds to assess ETC complex activities
405 of mitochondria. (j) Bar graph depicting C I, Complex II (CII), and CIV activities (k) Western blot
406 of mitochondrial ETC complex proteins and (l) densitometry analysis normalized to COXIV
407 levels. N=3 animals/ group. All data shown in mean ± SEM. P values were determined by
408 unpaired, two-tailed, Student T test, *P<0.05, **P<0.01.

409

410 # Discussion

411

412 We have previously demonstrated that dATP is a candidate myosin activator for heart failure
413 therapy and established that it can improve contraction and relaxation in a variety of heart
414 failure models[46,47]. However, an important question that needed to be addressed is whether
415 or how elevation of dATP affects cardiomyocyte (CM) metabolism. The present study
416 demonstrates that a modest elevation of dATP levels in CMs that is sufficient to improve LV and
417 CM function, also improves metabolism and cellular bioenergetics, providing crucial insights into
418 the relationship between energy supply-demand and crossbridge activity in CMs.
419
420 We employed novel strategies to stably overexpress RNR, utilizing ubiquitylation-resistant
421 variant RRM2B in a transgenic mice model (TgRRB) and found that dATP level was significantly
422 elevated from <0.1% to ~ 0.5-1% (of the total ATP pool) in TgRRB mouse heart (Fig. 1a, S2).
423 This novel strategy yielded important insights. First, it appears that this approach, to elevate
424 dATP with a proteolytically resistant variant RNR is limited to dATP content of ~1% of the total
425 ATP pool[48]. This relatively low-level elevation of dATP is sufficient to improve systolic as well
426 as diastolic function in the heart *in vivo* and in isolated CMs *in vitro*. Second, we demonstrated
427 that cells with elevated dATP have elevated basal oxygen consumption due to changes in
428 myosin state, independent of active crossbridge cycling. Third, these cells respond with a
429 metabolic shift, such that there are higher pools of oxidative metabolites, with elevated
430 OXPHOS, FAO, and energy generation in TgRRB-CMs. Finally, we provide evidence that the

431 long-term mitochondrial remodeling in CMs may occur to accommodate for the higher energy
432 demands of the high functioning dATP CMs.
433
434 The current study demonstrates that long-term elevation of cardiac [dATP] results in sustained
435 elevation of basal left ventricular performance while maintaining high workload and energetic
436 reserve, with no signs of hypertrophy or altered diastolic dimensions[23]. This is important
437 because in some cardiomyopathies with elevated workload, there is cellular hypertrophy along
438 with other pathological remodeling. The improved twitch function with no significant changes in
439 Ca^{2+} transient amplitude (Fig.1j and Table S2, S3), suggest differences in the cellular
440 contractility are due to dATP-mediated activation of myosin heads[20]. Interestingly, the skinned
441 myocardial force measurements revealed that there might be adaptation in the myosin structure
442 and function with chronic exposure to dATP elevation in TgRRB (Fig. S6). Nonetheless, TgRRB
443 samples did remain sensitive to dATP elevation leading to increased force generation. Cellular
444 relaxation kinetics are also improved, perhaps due to improved calcium decay kinetics (Fig. 1m)
445 and the maintenance of the myosin in its activated state during relaxation, which may further
446 facilitate subsequent contractions[22,49]. Thus, dATP increases myosin cycling and sarcomere
447 function without prolonging the systole (Fig.1, Table S2)[47,50] or shortening diastole, which
448 possibly makes it an energy-efficient myotrope.
449
450 In CMs, myosin is the primary mechanoenzyme coupling the energy released from ATP
451 hydrolysis to force generation. Biochemical studies have shown that myosin heads (S1, Fig. 3a)
452 are present in multiple physiological/conformational states in resting muscle, and these have
453 different rates of ATP consumption which, in turn, when modulated (pathological mutation) can
454 affect the overall CM metabolism[32,51]. Our recent study demonstrated that biochemically
455 dATP pushes myosin heads from a low ATP consumption (SRX) to higher ATP consumption
456 (DRX) state (Fig. 3a)[21]. Here we demonstrated that the dATP induced change in SRX/DRX
457 underlies the greater basal respiration of TgRRB-CMs (Fig. 3c). Thus, demonstrating that the
458 effect of dATP on basal energetics is by myosin state modulation.
459
460 In the present study, we also found that dATP elevation rewires cellular metabolism with to
461 avoid energy deficit and downstream pathology. Metabolomic analysis showed that dATP
462 elevation in TgRRB-CMs results higher OXPHOS with greater levels of pyruvate, FAO
463 metabolites (Fig 5c), TCA intermediates (Fig. 4), and anaplerotic metabolites (Fig. 5d), but not in
464 the levels of PPP metabolites (Fig. 4). The shift away from PPP to glycolysis might add to the

465 pyruvate accumulation. Alternatively, FAO may be responsible for filling up the TCA cycle
466 metabolites such that glycolysis needed is less and can cause pyruvate to build up. Overall,
467 TgRRb-CMs had a modest but significant increase in ATP levels (Fig. 5a). Interestingly, we also
468 found elevated levels of reducing agents (e.g., GSH/GSSG, NADH) indicating low oxidative
469 stress in high energy TgRRB-CMs (Fig. 5b).
470
471 The oxidative metabolic profile of the TgRRB-CMs is supported by high functioning
472 mitochondria displaying higher cristae density and number of ETC complexes and their activity
473 in TgRRB (Fig. 6f, j, l), indicating an improvement in mitochondrial intrinsic ATP synthesis
474 capacity in TgRRB-CMs[52]. This adaptation may be the consequence of a trade-off between
475 the elevated mechanical work (contraction), sarcomere architecture, and oxidative metabolic
476 power (OCR) as produced by mitochondria and serves as a mechanism for increasing
477 metabolic power without constraining contractile function. Thus, TgRRB-CMs show shift in
478 metabolism towards OXPHOS and high mitochondrial oxidative capacity to generate ATP,
479 thereby avoiding activation of anaerobic respiration observed in pathological condition[31,32].
480
481 In this manner, dATP mediated steady elevated cellular respiration does not compensate LV
482 contractile function– e.g., normalize pressure to WT levels – but remodels cellular metabolism in
483 the long run via more oxidative metabolism and increased mitochondrial turnover and ETC
484 activity. We showed that dATP-induced myosin activation elevates resting metabolism and
485 contractility in CMs; however, the mechanism behind how this elevated flux induces enhanced
486 OXPHOS and mitochondrial remodeling is unknown. TgRRb mice were lower in body weight
487 (Fig. S1) than WT littermates suggesting that the whole-body metabolic rate might be affected.
488 Intriguingly, dATP can be used as a tool to understand how cellular as well as body metabolism
489 responds to increased myosin cross bridge activity. Overall, TgRRB mice demonstrate
490 beneficial compensatory changes in CM metabolism to accommodate for the gain in ventricular
491 function.
492
493 In summary, we provide the first evidence that a small increase (~1%) dATP via persistent
494 overexpression of RNR variant promotes cardiac contractile function putatively by elevating
495 basal ATPase activity of myosin and adapts cellular metabolism towards higher oxidative
496 capacity. Elevated cellular and mitochondrial dATP (Fig. S2) has a panoply of beneficial effects
497 on cardiac metabolism, from remodeling of cellular metabolic pathways and respiration to

498 mitochondrial cristae alterations and function representing dATP as a potential therapeutic
499 option for targeting the contractile and metabolic deficit observed in heart diseases.
500
501 Study limitations
502
503 A limitation of the study is its dependence on isolated Langendorff-perfused hearts for
504 assessing cardiac function. Although isolated Langendorff-perfused heart preparation provides
505 a way to investigate heart function independent of the neurohumoral and physiological
506 adaptations, other physiological measurements can give more insights into the effect of
507 elevated dATP on other factors regulating cardiac function, like afterload. With long-term
508 exposure to dATP in this model, we did observe dATP-independent differences in force
509 generation, possibly indicating secondary effects of chronic elevation of contractility. Seahorse
510 assay and metabolomics in this study were performed on isolated CMs from TgRRB mice and
511 age-matched WT mice. This approach has the clear advantage of exclusively looking at the
512 effect of myotrope dATP on CM metabolites and energetics. However, it needs to be specified
513 that metabolism could be altered during CM isolation and time in culture during the assay. Also,
514 seahorse measurements are carried out on unloaded cells, which could affect the interpretation
515 of the energy consumption. Despite this limitation, we observed significant differences in the
516 metabolism and energetics of TgRRB-CMs and WT-CMs, emphasizing the independent
517 metabolic effects of dATP. Since all the measurements carried out in this study are in a healthy
518 heart, a critical next step is to study the metabolic consequence of dATP elevation in a stressed
519 heart. This enhanced understanding of the role of metabolic regulation in the heart via dATP
520 should open possibilities for harnessing these processes for therapeutic potential.

521

522
523
524
525

Materials and Methods

All animal experiments were approved by the University of Washington (UW) Animal Care Committee. Animals were cared for in accordance with the US National Institutes of Health Policy on Humane Care and Use of Laboratory Animals in the Department of Comparative Medicine at UW.

Echocardiography

Echocardiography was performed on mice at four months of age (Vevo 3100, Fujifilm Visual Sonics, Toronto, Canada) as previously described [23]. The parasternal short axis view at the mid-papillary level was used to obtain M-mode images for analysis of LV end-diastolic (LVEDD), end-systolic (LVESD) dimensions, fraction shortening (SF) and ejection fraction (EF). Diastolic function was assessed by measurement of trans mitral flow parameters, including systolic ejection time (SET) and isovolumic relaxation time (IVRT) from apical 4-chamber view with pulsed wave Doppler. Tissue Doppler imaging was performed by placing sample volume at the septal corner of the mitral annulus to measure early diastolic myocardial relaxation velocity (E'). All analysis was done by a blinded single reader.

Isolated perfused mouse heart preparation

Left ventricular contractile kinetics were measured in Langendorff isolated heart preparations as described previously [36]. Excised mouse hearts were perfused at a constant pressure of 80 mmHg in a modified Krebs-Henseleit buffer (In mM: 118 NaCl, 25 $NaHCO_3$, 5.3 KCl, 2.0 $CaCl_2$, 1.2 $MgSO_4$, 0.5 EDTA, 5.5 glucose, 0.5 sodium pyruvate, equilibrated with 95% O_2 and 5% CO_2, pH 7.4) at 37°C. After equilibration, baseline function was monitored at a fixed end-diastolic pressure of 8-10 mmHg for 10-20 minutes by way of a water-filled balloon inserted into the LV. Balloon volume was increased in 5 μL increments to determine the pressure-volume relationship in the myocardium. Finally, buffer [Ca^{2+}] was increased from 2mM to 4mM for 20 minutes to stimulate an increase in cardiac work.

Adult mouse cardiomyocyte isolation and contractile assessment

559 CMs were isolated from mice via enzymatic digestion through retrograde aortic perfusion as
560 described previously [23]. Briefly, hearts were rapidly excised, cannulated, and perfused with a
561 collagenase/protease solution, following which the ventricles were removed, minced, and
562 triturated. Contractile assessments of cells were made immediately after stepwise reintroduction
563 of calcium and incubation in Fura-2-AM (Invitrogen) to measure calcium transients. Cell
564 shortening and re-lengthening and calcium transients were measured at 1 Hz and 37°C using
565 an IonOptix µStep video recording system (IonOptix, Westwood, MA, USA). Measurements
566 were performed by four independent experimentalists and analyzed by the same reader. In
567 addition, we also measured Sarcoplasmic Reticulum (SR) Ca^{2+} load using the caffeine
568 technique. Briefly, isolated CMs will be loaded with Fluo-4 Ca2+ indicator dye, then paced (1
569 Hz for 8-10s) to stabilize Ca^{2+} transient amplitudes before pico-spritzing a 20 mM caffeine
570 solution.
571
572 dATP quantification in cardiac tissue
573
574 dATP content in CMs was measured by high-performance liquid chromatography-mass
575 spectrometry (HPLC-MS/MS) as described previously [53]. Freshly isolated whole mouse
576 ventricle or CMs were flash-frozen, stored at -80°C, and nucleotides were extracted 1-3 days
577 before measurement using a 50% methanol solution. The supernatant was stored at -20°C until
578 ready for injection into the HPLC-MS/MS system. ATP and dNTP standard curves were used to
579 calculate the concentration of each nucleotide. dATP content was then normalized to ATP in the
580 same samples.
581
582 Western blot
583
584 Protein samples were solubilized in 1% NP-40 lysis buffer with 4% protease inhibitors (Sigma)
585 and centrifuged for 14,000 g for 5 minutes. The supernatant was mixed with SDS protein
586 sample buffer containing β-mercaptoethanol (Bio-Rad) and resolved by SDS-PAGE on 4-20%
587 Mini-Protean GTX Stain-Free gels (Bio-Rad). Protein transfer to 0.45 mm polyvinylidene
588 difluoride membranes was performed at constant 100 volts at 4°C in Towbin's buffer containing
589 20% methanol for 1 hour. Blots were blocked for 1 hour at room temperature in 1x BlockerFL
590 (Thermo Scientific) before overnight incubation with primary antibodies (Total OXPHOS Rodent
591 WB Antibody Cocktail: Abcam ab110413, 1:500; Anti-COX IV antibody - Mitochondrial Loading
592 Control: Abcam ab16056, 1:500; Human RRM1: Abcam ab137114, 1:500; Human

593 RRM2/RRM2B: ThermoFisher PA579937, 1:1000 Human Rrm2B: ThermoFisher MA5-29529
594 1:1000, GAPDH: Fitzgerald 10R-2932 1:1000). One-hour incubation with StarBright fluorescent
595 secondary antibody (#12005866, #12004162 BIO-RAD) diluted 1:2500 in PBS-Tween 5% milk
596 was used to detect primary antibodies bound to the blot by BIO-RAD ChemiDoc imaging
597 system. The densitometry of western blots was performed using I Image Lab (BIO-RAD USA).
598
599 Enzyme Assays
600
601 Citrate synthase activity, a key enzyme in the Kreb's cycle that is commonly used marker for
602 mitochondrial mass, was measured on tissue homogenates and isolated CMs with a kit
603 purchased from Sigma-Aldrich (MAK193; St. Louis, MO, USA). In brief, CS activity is
604 determined using a coupled enzyme reaction, which results in a colorimetric (412 nm) product
605 proportional to the enzymatic activity present. We normalized the CS activity to the number of
606 cells used for the assay.
607
608 Metabolomic analysis
609
610 CMs samples were isolated from hearts of age matched (5-7 months) TgRRB and WT mice.
611 The CMs were either plated for XFe24 bioenergetic profiling or flash frozen for Metabolomic
612 analysis. Aqueous metabolites for targeted LC-MS analysis were extracted using a protein
613 precipitation method. Samples were first homogenized in 200 µL purified deionized water at 4
614 ˚C, and then 800 µL of methanol containing 6C13-glucose and 2C13-glutamate (reference
615 internal standards) was added. Afterwards, samples were vortexed, stored for 30 minutes at -20
616 ˚C, sonicated in an ice bath for 10 minutes, centrifuged for 15 min at 14,000 rpm and 4 ˚C, and
617 then 600 µL of supernatant was collected from each sample. Lastly, recovered supernatants
618 were dried on a SpeedVac and reconstituted in 1 mL of LC-matching solvent containing 2C13-
619 tyrosine and 3C13-lactate (reference internal standards). Protein pallets that were left over from
620 the sample prep were saved for the BCA protein assay.
621
622 Targeted LC-MS metabolite analysis was performed on a duplex-LC-MS system composed of
623 two Shimadzu UPLC pumps, CTC Analytics PAL HTC-xt temperature-controlled auto-sampler
624 and AB Sciex 6500+ Triple Quadrupole MS equipped with ESI ionization source. UPLC pumps
625 were connected to the auto-sampler in parallel and were able to perform two chromatography
626 separations independently from each other. Each sample was injected twice on two identical

627 analytical columns (Waters XBridge BEH Amide XP) performing separations in hydrophilic
628 interaction liquid chromatography (HILIC) mode. While one column was performing separation
629 and MS data acquisition in ESI+ ionization mode, the other column was getting equilibrated for
630 sample injection, chromatography separation and MS data acquisition in ESI- mode. Each
631 chromatography separation was 18 minutes (total analysis time per sample was 36 minutes).
632 MS data acquisition was performed in multiple-reaction-monitoring (MRM) mode. LC-MS system
633 was controlled using AB Sciex Analyst 1.6.3 software. Measured MS peaks were integrated
634 using AB Sciex MultiQuant 3.0.3 software. 205 metabolites and 4 reference standards were
635 measured in the study samples. In addition to the study samples, two sets of quality control
636 (QC) samples were used to monitor the assay performance as well as data reproducibility. One
637 QC [QC(I)] was a pooled human serum sample used to monitor system performance, and the
638 other QC [QC(S)] was pooled study samples, and this QC was used to monitor data
639 reproducibility. The data were well reproducible, with average and median CVs of 5.2% and
640 4.3%, respectively. Generated MS data were normalized vs BCA total protein count. The PCA
641 and pathway impact analysis of the metabolomic data were carried out using MetaboAnalyst 5.0
642 software. The fold change calculated for the metabolite ratios (Lactate/Pyruvate,
643 phosphocreatine (pCr)/ATP, NAD^+/NADH, and GSH/GSSG) are normalized to the WT group.
644 Differences in the abundance of individual metabolites were determined using a student's t test
645 (two-tailed, unpaired comparison). A value of $P < 0.05$ was considered statistically significant.
646 Data are given as mean ± SEM.
647
648 XFe24 bioenergetic profiling.
649
650 Isolated CMs were seeded on matrix gel–coated cell culture microplates (Agilent Seahorse
651 XF24) at the cell intensity of 20000 cells/well. Generally, before performing the experiment, the
652 culture medium was changed into 625uL assay medium (Agilent Seahorse XF Base Medium),
653 and then, cells were incubated in 37°C non-CO2 incubator for 1 hour.
654
655 The bioenergetic response of cardiomyocytes (CMs) was measured with the Seahorse
656 Bioscience XFe24 Flux Analyzer. For oxygen consumption rate (OCR) measurements, the
657 plating media were changed to 675 μl DMEM-based Seahorse (Agilent, 102353-100)
658 supplemented with 4 mmol/l glutamine, 1 mmol/l pyruvate and 5 mmol/l glucose 1 h before
659 assay. The XFe24 automated protocol consisted of 10 min delay following microplate insertion,
660 baseline OCR measurements [3 times (3 min mix, 2 min wait, 3 min measure)], followed by

661 injection of port A (75 μl). The same protocol is followed for the port B (75 μl) and port C (75 μl).
662 Optimal concentrations of oligomycin (Sigma, 75351), carbonyl cyanide-p-
663 trifluoromethoxyphenylhydrazone (FCCP; Sigma, C2920), Rotenone (Sigma, R8875) and
664 antimycin A (Sigma, A6874) were diluted in DMSO (Sigma, 154938). XF measures the oxygen
665 consumption rate (OCR), represents mitochondrial respiration. The OCR measurements were
666 normalized to the protein concentration. Experimental replicates were normalized to protein
667 concentration. Optimization of seeding density was conducted in compliance with the Seahorse
668 XF24 manufacturer recommendations through multiple experiments to identify a cell count that
669 provided basal OCR readings sufficiently above background, within tested linear response
670 ranges and with full re-oxygenation of the media attained between measurements.
671
672 Transmission Electron Microscopy
673
674 Tissue samples were fixed overnight in ½ strength Karnovsky's (2%paraformaldehyde/2.5%
675 glutaraldehyde buffered with 0.2M cacodylate) and post fixed in 2% OsO4 buffered in 0.2M
676 cacodylate buffer. After dehydration, tissues were embedded in Epon 812 (Electron Microscopy
677 Sciences), thin sectioned (70 nm), and stained with uranyl acetate for 2 h and lead citrate for 5
678 min. The samples were imaged using a JEOL 1230 transmission electron microscope set to 80
679 kV, and the images were captured using a Gatan digital imaging system. n≥4 scans were taken
680 per animals per magnification. Mitochondrial objects in the images were pre-segmented in an
681 automated manner using ImageJ software: after noise reduction by repetitively convolving each
682 image with a Gaussian function, images were thresholded by the 'Percentile' auto thresholding
683 method. Boundaries between background and foreground were smoothened by repeated
684 erosion and dilation. Lastly, particles were identified based on set cut offs for size and
685 circularity. Results from this initial machine-based analysis were subsequently manually verified
686 as mitochondrial particles in a blinded fashion. Image coordinates of each identified particle
687 were used for the subsequent calculation of mitochondrial number, size, aspect ratio, while
688 brightness provided an estimate for cristae density as described in [54].
689
690 Statistics
691

692 The statistical analyses were performed using GraphPad Prism 8 (Graphpad Software). Results
693 were considered statistically significant at $p \leq 0.05$. The results shown here are mean ± SEM
694 unless otherwise stated.
695

696 Acknowledgements

697

698 We acknowledge Dr. Kristina B. Kooiker for her guidance and assistance with trabeculae force
699 measurement and sarcomeric protein phosphorylation protocol. KM was funded by the Institute
700 for Stem Cells and Regenerative Medicine fellows' program. MR acknowledges NIH R01
701 HL128368, P30 AR074990 and, DOD MD170031. FMH acknowledges NIH Grant K08
702 HL128826 and the Locke Charitable Trust.
703
704
705

References

1. Lopaschuk GD, Karwi QG, Tian R, Wende AR, Abel ED. Cardiac Energy Metabolism in Heart Failure. Circ Res [Internet]. 2021 May 14 [cited 2021 Sep 3];128:1487–513.
2. Psotka MA, Gottlieb SS, Francis GS, Allen LA, Teerlink JR, Adams KF, et al. Cardiac Calcitropes, Myotropes, and Mitotropes: JACC Review Topic of the Week [Internet]. Vol. 73, Journal of the American College of Cardiology. Elsevier USA; 2019 [cited 2022 Mar 2]. p. 2345–53.
3. Ahmad T, Miller PE, McCullough M, Desai NR, Riello R, Psotka M, et al. Why has positive inotropy failed in chronic heart failure? Lessons from prior inotrope trials. Eur J Heart Fail. 2019;21(9):1064–78.
4. Shah KS, Xu H, Matsouaka RA, Bhatt DL, Heidenreich PA, Hernandez AF, et al. Heart Failure With Preserved, Borderline, and Reduced Ejection Fraction. J Am Coll Cardiol. 2017 Nov;70(20):2476–86.
5. Yancy CW, Jessup M, Bozkurt B, Butler J, Casey DE, Drazner MH, et al. 2013 ACCF/AHA Guideline for the Management of Heart Failure. J Am Coll Cardiol. 2013 Oct;62(16):e147–239.
6. Virani SS, Alonso A, Benjamin EJ, Bittencourt MS, Callaway CW, Carson AP, et al. Heart Disease and Stroke Statistics—2020 Update: A Report From the American Heart Association. Circulation [Internet]. 2020 Mar 3 [cited 2020 Apr 27];141(9):e139–596.
7. Vigen R, Maddox TM, Allen LA. Aging of the United States population: impact on heart failure. Curr Heart Fail Rep. 2012 Dec;9(4):369–74.
8. Teerlink JR, Diaz R, Felker GM, McMurray JJV, Metra M, Solomon SD, et al. Cardiac Myosin Activation with Omecamtiv Mecarbil in Systolic Heart Failure. NEJM [Internet]. 2020 Nov 13 [cited 2021 Oct 10];384(2):105–16.
9. Bakkehaug JP, Kildal AB, Engstad ET, Boardman N, Næsheim T, Rønning L, et al. Myosin activator omecamtiv mecarbil increases myocardial oxygen consumption and impairs cardiac efficiency mediated by resting myosin ATPase activity. Circ Hear Fail [Internet]. 2015 May 1 [cited 2022 Mar 12];8(4):766–75.
10. Kinoshita Y, Nishigaki K. Unexpectedly general replaceability of ATP in ATP-requiring enzymes. J Biochem. 1997 Jul;122(1):205–11.
11. Regnier M, Homsher E. The effect of ATP analogs on posthydrolytic and force development steps in skinned skeletal muscle fibers. Biophys J. 1998 Jun;74(6):3059–71.

739 12. Regnier M, Martyn DA, Chase PB. Calcium regulation of tension redevelopment kinetics
740 with 2-deoxy-ATP or low [ATP] in rabbit skeletal muscle. Biophys J. 1998
741 Apr;74(4):2005–15.
742 13. Regnier M, Lee DM, Homsher E. ATP Analogs and Muscle Contraction : Mechanics and
743 Kinetics of Nucleoside Triphosphate Binding and Hydrolysis. Biophys J [Internet].
744 1998;74(6):3044–58.
745 14. Moussavi-Harami F, Razumova M V., Racca AW, Cheng Y, Stempien-Otero A, Regnier
746 M. 2-Deoxy adenosine triphosphate improves contraction in human end-stage heart
747 failure. J Mol Cell Cardiol. 2015;79:256–63.
748 15. Lundy SD, Murphy SA, Dupras SK, Dai J, Murry CE, Laflamme MA, et al. Cell-based
749 delivery of dATP via gap junctions enhances cardiac contractility. J Mol Cell Cardiol.
750 2014;
751 16. Nowakowski SG, Regnier M, Daggett V. Molecular mechanisms underlying deoxy-ADP.Pi
752 activation of pre-powerstroke myosin. Protein Sci [Internet]. 2017 Apr [cited 2019 May
753 19];26(4):749–62.
754 17. Regnier M, Martin H, Barsotti RJ, Rivera AJ, Martyn DA, Clemmens E. Cross-bridge
755 versus thin filament contributions to the level and rate of force development in cardiac
756 muscle. Biophys J. 2004;87(3):1815–24.
757 18. Regnier M, Rivera AJ, Chen Y, Chase PB. 2-deoxy-ATP enhances contractility of rat
758 cardiac muscle. Circ Res. 2000;86(12):1211–7.
759 19. Nowakowski SG, Regnier M, Daggett V. Molecular mechanisms underlying deoxy-ADP.Pi
760 activation of pre-powerstroke myosin. Protein Sci [Internet]. 2017 Apr 1 [cited 2020 Sep
761 20];26(4):749–62.
762 20. Powers JD, Yuan CC, McCabe KJ, Murray JD, Childers MC, Flint G V., et al. Cardiac
763 myosin activation with 2-deoxy-ATP via increased electrostatic interactions with actin.
764 Proc Natl Acad Sci U S A [Internet]. 2019 Jun 4 [cited 2020 Sep 20];166(23):11502–7.
765 21. Walklate J, Kao K, Regnier M, Geeves MA. Exploring the super-relaxed state of myosin
766 in myofibrils from fast-twitch, slow-twitch, and cardiac muscle. J Biol Chem [Internet].
767 2022 Jan [cited 2022 Feb 7];298(3):101640.
768 22. Ma W, Childers M, Murray J, Moussavi-Harami F, Gong H, Weiss R, et al. Myosin
769 dynamics during relaxation in mouse soleus muscle and modulation by 2′-deoxy-ATP. J
770 Physiol [Internet]. 2020 Nov 1 [cited 2021 Sep 24];598(22):5165–82.
771 23. Nowakowski SG, Kolwicz SC, Korte FS, Luo Z, Robinson-Hamm JN, Page JL, et al.
772 Transgenic overexpression of ribonucleotide reductase improves cardiac performance.

773 Proc Natl Acad Sci. 2013;110(15):6187–92.
774 24. Kolwicz SC, Odom GL, Nowakowski SG, Moussavi-Harami F, Chen X, Reinecke H, et al.
775 AAV6-mediated cardiac-specific overexpression of ribonucleotide reductase enhances
776 myocardial contractility. Mol Ther. 2016;24(2):240–50.
777 25. Thomson KS, Odom GL, Murry CE, Mahairas GG. Translation of Cardiac Myosin
778 Activation. J Am Coll Cardiol. 2016;1(7):666–79.
779 26. Qiu W, Zhou B, Darwish D, Shao J, Yen Y. Characterization of enzymatic properties of
780 human ribonucleotide reductase holoenzyme reconstituted in vitro from hRRM1, hRRM2,
781 and p53R2 subunits. Biochem Biophys Res Commun. 2006 Feb;340(2):428–34.
782 27. Yen Y, Chu B, Yen C, Shih J, Zhou B. Enzymatic property analysis of p53R2 subunit of
783 human ribonucleotide reductase. Adv Enzyme Regul. 2006 Sep;46(1):235–47.
784 28. Cho EC, Kuo ML, Cheng JH, Cheng YC, Hsieh YC, Liu YR, et al. RRM2B-mediated
785 regulation of mitochondrial activity and inflammation under oxidative stress. Mediators
786 Inflamm. 2015 May;2015:287345.
787 29. Xue L, Zhou B, Liu X, Wang T, Shih J, Qi C, et al. Structurally dependent redox property
788 of ribonucleotide reductase subunit p53R2. Cancer Res. 2006 Oct;66(4):1900–5.
789 30. Liu X, Xue L, Yen Y. Redox property of ribonucleotide reductase small subunit M2 and
790 p53R2. Methods Mol Biol. 2008;477:195–206.
791 31. Ranjbarvaziri S, Kooiker KB, Ellenberger M, Fajardo G, Zhao M, Vander Roest AS, et al.
792 Altered Cardiac Energetics and Mitochondrial Dysfunctionin Hypertrophic
793 Cardiomyopathy. Circulation [Internet]. 2021 Nov 23 [cited 2021 Nov 26];144:1714–31.
794 32. Toepfer CN. Myosin Sequestration Regulates Sarcomere Function , Cardiomyocyte
795 Energetics , and Metabolism , Informing the Pathogenesis of Hypertrophic
796 Cardiomyopathy. Circulation [Internet]. 2020 [cited 2020 Jan 27];
797 33. Vitale G, Ferrantini C, Piroddi N, Scellini B, Pioner JM, Colombini B, et al. The relation
798 between sarcomere energetics and the rate of isometric tension relaxation in healthy and
799 diseased cardiac muscle. J Muscle Res Cell Motil [Internet]. 2021;42(1):47–57.
800 34. Roest AS Vander, Liu C, Morck MM, Kooiker KB, Jung G, Song D, et al. Hypertrophic
801 cardiomyopathy ß-cardiac myosin mutation (P710R) leads to hypercontractility by
802 disrupting super-relaxed state. bioRxiv [Internet]. 2020 [cited 2021 Jan
803 8];2020.11.10.375493.
804 35. Psotka MA, Gottlieb SS, Francis GS, Allen LA, Teerlink JR, Adams KF, et al. Cardiac
805 Calcitropes, Myotropes, and Mitotropes: JACC Review Topic of the Week [Internet]. Vol.
806 73, Journal of the American College of Cardiology. American College of Cardiology

807 FoundationWashington, D.C.; 2019 [cited 2022 Sep 19]. p. 2345–53.
808 36. Kolwicz SC, Hall JK, Moussavi-Harami F, Chen X, Hauschka SD, Chamberlain JS, et al.
809 Gene Therapy Rescues Cardiac Dysfunction in Duchenne Muscular Dystrophy Mice by
810 Elevating Cardiomyocyte Deoxy-Adenosine Triphosphate. JACC Basic to Transl Sci
811 [Internet]. 2019 Oct [cited 2019 Oct 8];
812 37. Powers JD, Kooiker KB, Mason AB, Teitgen AE, Flint G V., Tardiff JC, et al. Modulating
813 the tension-time integral of the cardiac twitch prevents dilated cardiomyopathy in murine
814 hearts. JCI Insight [Internet]. 2020 Oct 15 [cited 2022 Sep 20];5(20).
815 38. Powers JD, Williams CD, Regnier M, Daniel TL. A Spatially Explicit Model Shows How
816 Titin Stiffness Modulates Muscle Mechanics and Energetics. Integr Comp Biol [Internet].
817 2018 Aug 1 [cited 2022 Oct 3];58(2):186–93.
818 39. Nag S, Trivedi D V. To lie or not to lie: Super-relaxing with myosins [Internet]. Vol. 10,
819 eLife. eLife Sciences Publications, Ltd; 2021 [cited 2021 Dec 29]. p. 1–21.
820 40. Walklate J, Kao K, Regnier M, Geeves MA. Exploring the Super-relaxed State of Myosin
821 in Myofibrils from Fast-twitch, Slow-twitch and Cardiac Muscle. J Biol Chem.
822 2022;101640.
823 41. Hill BG, Dranka BP, Zou L, Chatham JC, Darley-Usmar VM. Importance of the
824 bioenergetic reserve capacity in response to cardiomyocyte stress induced by 4-
825 hydroxynonenal. Biochem J [Internet]. 2009 Nov 15 [cited 2021 Sep 3];424(1):99–107.
826 42. Gollapudi SK, Ma W, Chakravarthy S, Combs AC, Sa N, Langer S, et al. Two Classes of
827 Myosin Inhibitors, Para-nitroblebbistatin and Mavacamten, Stabilize β-Cardiac Myosin in
828 Different Structural and Functional States. J Mol Biol [Internet]. 2021 [cited 2021 May
829 10];433(23).
830 43. Shao D, Kolwicz SC, Wang P, Roe ND, Villet O, Nishi K, et al. Increasing Fatty Acid
831 Oxidation Prevents High-Fat Diet-Induced Cardiomyopathy Through Regulating Parkin-
832 Mediated Mitophagy. Circulation [Internet]. 2020 Sep 8 [cited 2022 Sep 2];142(10):983–
833 97.
834 44. Fajardo G, Coronado M, Matthews M, Bernstein D. Mitochondrial Quality Control in the
835 Heart: The Balance between Physiological and Pathological Stress [Internet]. Vol. 10,
836 Biomedicines. Biomedicines; 2022 [cited 2022 Sep 24].
837 45. Zhou B, Wang DDH, Qiu Y, Airhart S, Liu Y, Stempien-Otero A, et al. Boosting NAD level
838 suppresses inflammatory activation of PBMCs in heart failure. J Clin Invest [Internet].
839 2020 [cited 2021 Jul 5];130(11):6054–63.
840 46. Kolwicz SC, Odom GL, Nowakowski SG, Moussavi-Harami F, Chen X, Reinecke H, et al.

841 AAV6-mediated cardiac-specific overexpression of ribonucleotide reductase enhances
842 myocardial contractility. Mol Ther. 2016;24(2):240–50.
843 47. Kadota S, Carey J, Reinecke H, Leggett J, Teichman S, Laflamme MA, et al.
844 Ribonucleotide reductase-mediated increase in dATP improves cardiac performance via
845 myosin activation in a large animal model of heart failure. Eur J Heart Fail. 2015;17:772–
846 81.
847 48. Zimanyi CM, Chen PYT, Kang G, Funk MA, Drennan CL. Molecular basis for allosteric
848 specificity regulation in class ia ribonucleotide reductase from Escherichia coli. Elife. 2016
849 Jan 12;5(JANUARY2016).
850 49. McCabe KJ, Aboelkassem Y, Teitgen AE, Huber GA, McCammon JA, Regnier M, et al.
851 Predicting the effects of dATP on cardiac contraction using multiscale modeling of the
852 sarcomere. Arch Biochem Biophys [Internet]. 2020 Nov 30 [cited 2021 Feb 3];695.
853 50. Woody MS, Greenberg MJ, Barua B, Winkelmann DA, Goldman YE, Ostap EM. Positive
854 cardiac inotrope omecamtiv mecarbil activates muscle despite suppressing the myosin
855 working stroke. Nat Commun [Internet]. 2018 Dec 21 [cited 2019 May 23];9(1):3838.
856 51. Wilson C, Naber N, Cooke R. The role of the super-relaxed state of myosin in human
857 metabolism. Metab Open [Internet]. 2021 [cited 2021 Sep 29];9:100068.
858 52. Karamanlidis G, Bautista-Hernandez V, Fynn-Thompson F, Del Nido P, Tian R. Impaired
859 mitochondrial biogenesis precedes heart failure in right ventricular hypertrophy in
860 congenital heart disease. Circ Hear Fail. 2011;4(6):707–13.
861 53. Olafsson S, Whittington D, Murray J, Regnier M, Moussavi-Harami F. Fast and sensitive
862 HPLC–MS/MS method for direct quantification of intracellular deoxyribonucleoside
863 triphosphates from tissue and cells. J Chromatogr B Anal Technol Biomed Life Sci
864 [Internet]. 2017;1068–1069(October):90–7.
865 54. Nielsen J, Gejl KD, Hey-Mogensen M, Holmberg HC, Suetta C, Krustrup P, et al.
866 Plasticity in mitochondrial cristae density allows metabolic capacity modulation in human
867 skeletal muscle. J Physiol. 2017 May 1;595(9):2839–47.
868